Published in final edited form as:
Nature. 2015 September 24; 525(7570): 548–551. doi:10.1038/nature14981.

Crystal structures of a double-barrelled fluoride ion channel

Randy B. Stockbridge[1], **Ludmila Kolmakova-Partensky**[1], **Tania Shane**[1], **Akiko Koide**[2], **Shohei Koide**[2], **Christopher Miller**[1,3], and **Simon Newstead**[4]

[1]Department of Biochemistry, Howard Hughes Medical Institute, Brandeis University, Waltham, MA 02454

[2]Department of Biochemistry and Molecular Biology, University of Chicago, Chicago, IL 60637

[3]Department of Physiology, Anatomy, and Genetics, University of Oxford, Oxford OX13QU, UK

[4]Department of Biochemistry, University of Oxford, Oxford OX13QU, UK

Abstract

To contend with hazards posed by environmental fluoride, microorganisms export this anion through F^--specific ion channels of the Fluc family1–4. Since the recent discovery of Fluc channels, numerous idiosyncratic features of these proteins have been unearthed, including extreme selectivity for F^- over Cl^- and dual-topology dimeric assembly5–6. To understand the chemical basis for F^- permeation and how the antiparallel subunits convene to form a F^--selective pore, we solved crystal structures of two bacterial Fluc homologues in complex with three different monobody inhibitors, with and without F^- present, to a maximum resolution of 2.1 Å. The structures reveal a surprising “double-barrelled” channel architecture in which two F^- ion pathways span the membrane and the dual-topology arrangement includes a centrally coordinated cation, most likely Na^+. F^- selectivity is proposed to arise from the very narrow pores and an unusual anion coordination that exploits the quadrupolar edges of conserved phenylalanine rings.

The fluoride anion, ubiquitous in the aqueous biosphere throughout evolutionary time, is a xenobiotic inhibitor of essential phosphoryl-transfer enzymes7. Unicellular organisms directly exposed to environmental F^- counteract the anion’s toxicity through the action of F^--exporting membrane transport proteins that keep cytoplasmic F^- below inhibitory levels1–4,8. Two recently discovered, phylogenetically unrelated families of F^- exporters carry out this task: the CLC^F F^-/H^+ antiporters, a strictly bacterial clade of the CLC superfamily of anion-transporters, and small membrane proteins of the Fluc family (also denoted crcB or FEX). Fluc genes are also found in plants, primitive marine chordates, and sponges, but not

Author contributions

RS, SN & CM performed experiments, analysed the data and wrote the paper. LP & TS performed experiments. SK & AK: Provided monobody clones and wrote paper.

Author Information

Coordinate files have been uploaded to the Protein Data Bank with PDB codes 5a40, 5a41 and 5a43 for the Bpe-S7, Bpe-L2 and Ec2-S9 complexes respectively. Correspondence and requests for materials should be addressed to Simon Newstead (simon.newstead@bioch.ox.ac.uk). The authors declare no competing financial interests. Reprints and permissions information is available at www.nature.com/reprints

Europe PMC Funders Author Manuscripts

in higher animals. We recently established5,6 that Fluc proteins are ion channels with two unusual properties: an exceedingly high specificity (>10^4) for F^- over Cl^-, and a dual-topology dimeric architecture, in which the two subunits forming the active channel associate in antiparallel transmembrane orientation. Dual-topology dimeric construction is known in small multidrug transporters9–11 but has not been previously observed in ion channels. These inferences regarding function and structure of Flucs provoke fundamental questions about their mechanisms. How does the channel achieve such extreme selectivity for F^-, arguably the highest selectivity of any ion channel? Does the protein contain a single pore on the subunit interface or two pores, one in each subunit, as with CLC Cl^- channels12? Is the channel homodimer symmetrical, or do the two subunits adopt different conformations, as in the multidrug resistance transporter EmrE9,11?

In previous work, the antiparallel transmembrane topology of Fluc channels was intimated by the distribution of positively charged residues in Fluc sequences13, was strongly suggested by crosslinking and functional reconstitution5, and was established definitively by two-sided block of single channels by “monobodies,” engineered proteins selected as high-affinity binding partners from combinatorial libraries6. We now use these monobodies in crystallization trials to form complexes with a Fluc channel from *Bordetella pertussis*, nicknamed Bpe5. Crystals could not be grown unless monobodies were present; however diffraction to 3.6 Å Bragg spacing was obtained with monobody Mb(Bpe-S7)6, hereafter denoted S7. A structure was solved, with phases initially determined by single-wavelength anomalous diffraction (SAD) of Bpe labelled with Hg at a unique cysteine residue, and improved with Hg-labelled selenomethionine-substituted samples (Extended Data Table 1). A view of the crystal lattice highlights the importance of the monobodies as crystallization chaperones, which exclusively mediate crystal contacts in all structures presented here (Extended Data Fig. 1).

Though devoid of F^- ions and of low resolution, the Bpe-S7 structure reveals the channel’s overall architecture (Fig. 1a). Bpe is an antiparallel homodimer in which each subunit consists of four transmembrane helices with an overall fold novel among membrane proteins. The 1700 $Å^2$ dimer interface is almost completely membrane-embedded. The third, highly conserved helix (TGxxxGLTTFSTFxxxE) is broken into two halves, TM3a and TM3b, by a 6-residue non-helical segment located roughly at the membrane’s center. These two segments, one from each subunit, cross each other near the channel’s twofold axis running parallel to the membrane plane. The channel is hourglass-shaped, with wide vestibules symmetrically opening to the two aqueous solutions (Fig. 1b) separated by a solid plug of protein 10-15 Å thick. A conspicuous, universally conserved TM1 arginine residue (R23) protrudes into each vestibule, suggestive of an electrostatic lure for F^-. No aqueous pore connecting the vestibules is visible in this low-resolution structure.

The protein is capped on both ends by the S7 monobody (Fig. 1c). This monobody was selected from a library designed to target convex protein surfaces14, and indeed its interaction surface, consisting largely of the residues diversified in the library, wraps around a protrusion formed from the channel’s TM1-TM2 and TM3b-TM4 connecting loops. An 8-residue loop on the monobody plunges deeply into each vestibule, contacting the channel mainly via side chains. Channel-monobody interactions are mostly hydrophobic, aromatic,

and H-bonding, the paucity of salt-bridges rationalizing the rather weak ionic strength dependence of monobody binding15. Most of the channel's aqueous-exposed surface is covered by monobody, consistent with S7 block of Bpe seen in single-channel recordings (Fig. 1c).

It is tempting to imagine that a central pore connects the two vestibules in an unseen "open" conformation. But the structure's low resolution and the absence of F^- preclude identification of the ion-permeation pathway. We therefore attempted *in meso* crystallization in hopes of identifying bound F^- ions. Crystals diffracting to 2.1 Å in the presence of 20 mM F^- were obtained with a different monobody, L2, also a blocker (Extended Data Fig. 2). Structures solved by molecular replacement (Extended Data Table 1) again show the channel with a monobody on each end (Extended Data Fig. 1 & 2). The channel's backbone conformation is identical to that in the lower-resolution structure (Cα rmsd 0.4 Å), and L2, though binding in an orientation different from S7's, also extends a long loop 8-10 Å into the vestibule, occluding much of the channel's water-exposed surface.

This higher-resolution structure alerts us to five intriguing electron densities (Fig. 2a & Extended Data Fig. 3). First, a prominent density located in the center of the plug separating the vestibules, precisely on the homodimer's twofold noncrystallographic axis (Fig. 2b). We identify this as a Na^+ ion on the basis of its coordination by four backbone carbonyl groups from residues in each subunit associated with the conserved TM3 break (G77, T80). This coordination is inconsistent with a F^- ion, a water, a divalent metal, or a K^+ ion16,17. Although coordination by only four oxygen ligands is uncommon for Na^+, it is nevertheless seen in ~15% of Na^+-binding sites in the protein database18. This deeply buried cation could not exchange with aqueous solution if the plug remains intact during functional activity, and indeed, Bpe channels with familiar behavior are readily recorded in solutions with Na^+ completely substituted by N-methyl glucamine (Extended Data Fig. 4). We conjecture that the ion is an important structural component incorporated irreversibly upon dimer assembly.

A second notable detail in the Bpe-L2 structure is a set of four electron densities located in crevices between TM2, TM3b, and TM4 near the channel's periphery, distant from the vestibules and the central plug (Fig. 2a,c). We provisionally identify these as F^- ions, labelled F1 and F2 in noncrystallographic symmetry-related pairs, according to their distinct chemical environments. The putative liganding atoms embracing these densities are consistent with a halide coordination shell. In particular, the surround is composed of electropositive side chains, which would engage the F^- ion's strong H-bond accepting tendencies. Prominent among these are a strongly conserved asparagine (N43) in TM2 and two conserved serines (S108, S112) in TM4. In addition, two pairs of conserved phenylalanine rings (F82, F85) near the TM3 break approach these densities in a telling side-on orientation that presents the electropositive carbons of the quadrupolar ring to the F^- ion. These four aromatic rings appear to be mutually stabilized in a striking "box" assembly. Edge-on aromatic liganding of anions is rare but not unprecedented in proteins19, and F^- coordination by aromatic edges appears in many small-molecule structures20. This type of coordination is reminiscent of the phenylalanine rings of a proposed Cl^--binding site in the bestrophin channel21. With a deficit of H-bond acceptors, the coordination shells observed

here would be chemically inimical to ordered waters, which cannot be distinguished from F^- based on x-ray scattering alone.

The two F^- ions of each pair lie in a vertical line tilted slightly off normal to the membrane plane, and so might mark a narrow permeation pathway. If these densities do indeed represent F^-, then their positions lead to a surprising conclusion: that the Bpe channel contains two pores running in antiparallel orientation along opposite sides of the dimer, rather than a single central pore connecting the vestibules through the plug. Two-pore behavior is not apparent in single-channel recordings since both are nearly always open5. The structures here would represent the monobody-blocked state similar to that observed electrophysiologically6,15.

Our reading of the structure as a double-barrelled channel depends crucially on identifying the four densities above as F^- ions. However, we do not consider the above evidence sufficiently strong to accept such an unusual picture as firmly established. Accordingly, two additional experimental approaches were pursued. First, a structure was determined for a different Fluc homologue, Ec2, complexed with a monobody S9 (Extended Data Fig. 5). This homologue of only 33% identity shows similar electrophysiological behavior to Bpe and is blocked by S9 at nanomolar concentrations6. Ec2-S9 crystals diffracting to 2.6 Å were grown from detergent in the presence of F^-, and to avoid model bias a structure was solved using SAD phasing with selenomethionine-labelled protein (Extended Data Table 1). The Ec2 and Bpe folds are identical (Cα rmsd 0.6 Å), with inferred Na^+ density appearing in equivalent locations. Two strong difference densities lie at precisely the same locations as the F1 ions in Bpe, coordinated identically (Fig. 3a). The appearance of these densities, in a separate homologue under very different crystallization conditions, strengthens our hypothesis that the four densities in Bpe represent F^- ions. Additional densities also appear in Ec2 in the general vicinity as the F2 ions in Bpe, but at this lower resolution and without supporting experimental evidence, these densities in Ec2 cannot be unambiguously assigned.

The chemical nature of the crevices housing the densities makes sense for narrow diffusion pathways welcoming to F^- ions in both homologs (Fig. 3b). In particular, the crevice-facing surface of TM4 is lined with H-donating side chains, as manifested by every fourth residue in the sequences of Bpe (Y104, S108, S112, T116) or Ec2 (S102, H106, S110, T114). These particular residues are only modestly conserved among Fluc channels, but H-bond donors reliably appear here throughout the family. These could plausibly contribute to a polar track along which largely dehydrated F^- ions move across the membrane. Because these pathways are extremely narrow, protein dynamics may be necessary to allow F^- permeation and of course the monobodies might force a conformation in which the two pores are less ‘open’ than in the fully conducting state.

We next examined the functional consequences of mutating each of three conserved Bpe residues coordinating the F^- densities: F82, F85, and N43. We did not observe single-channel activity in electrical recordings, but more sensitive “anion-dump” experiments22,23 reveal dramatic changes in F^- permeation (Fig. 3c). In these experiments, Bpe-reconstituted liposomes loaded with KF are suspended in low-F^- solutions, and the rate of passive F^- efflux is followed electrochemically. To eliminate the aromatic quadrupole, the conserved

phenylalanine residues were mutated individually to isoleucine. For F85I and F82I, efflux of F^- is 2 and 3 orders of magnitude slower, respectively, than for wild type (~$3x10^5$ s^{-1})15 (Extended Data Table 2). These mutations preserve the channel's integrity, since F^- efflux is blocked 50-80% by 6μM monobody (Extended Data Fig. 6). Strong selectivity against Cl^- is observed in parallel experiments with this sister-halide.

The conserved asparagine was substituted so as to alter or remove H-bonding capability (N43S, N43A), or to place an isosteric carboxylate at this position (N43D). The first two mutants were biochemically intractable, but N43D produces stable protein. Under standard conditions at pH 7, N43D supports robust, F^--selective efflux (Fig. 3d, Extended Data Table 2). We had envisioned that an anionic carboxylate at this position would prevent F^- entry into the channel. It is possible, however, that the pK_a of this group is perturbed upwards by its local environment, so that at neutral pH the carboxyl acts as a protonated surrogate for the N43 amide. The N43D mutant was therefore examined at several pH values. In stark contrast to the pH-independent activity of wild type Bpe and the F85I mutant (Extended Data Fig. 5), F^- efflux in N43D falls with increasing pH and is extinguished at pH 9 (Fig. 3d), verifying a key role of the H-bond donating N43 side chain in F^- conduction.

These mutagenic manipulations of F^- permeation add mechanistic evidence that argues strongly for assigning F^- ions to the densities in question. This inference makes it difficult to resist the conclusion that Flucs are double-barrelled F^- channels, with the observed F^- ions marking the ion-selective pathways. The two pathways are not segregated to each subunit as in CLC channels24; instead each pore comprises side chains from TM2, TM3b, and TM4 of one subunit plus the TM3-break phenylalanine from the opposing subunit. Though unexpected, this idea does not clash with any electrophysiological experiments, and double-pore assembly was explicitly cited previously as a possible though unlikely architecture consistent with the channel's functional behaviour5.

Two-pore assembly neatly accounts for evolutionary drift in eukaryotic Fluc channels, all of which consist of an inverted repeat of two homologous Fluc domains fused into a single polypeptide4,5. Alignments (Extended Data Fig. 7) show that "pore-2," where most residues arise from the C-terminal domain, retains the strict sequence conservation typical of the homodimeric bacterial Flucs, while the equivalent residues of "pore-1," mostly in the N-terminal domain, are far less conserved, notably along the TM4 polar track. This pattern is further confirmed for the two conserved phenylalanines, which from the same domain contribute to alternate pores. Thus, in pore-2, the strongly conserved equivalents of F82 project from the N-terminal domain and of F85 from the C-terminal domain, in dramatic contrast to their poorly conserved residue-twins contributing to pore-1. These sequence-based considerations suggest that pore-2 alone fulfills the F^--export function in eukaryotic Flucs. Recent experiments buttress this idea by showing that mutations of several C-terminal domain residues in pore-2 produce F^- hypersensitivity in yeast, whereas mutations of N-terminal domain, pore-1 counterparts are relatively harmless4. These features chronicle an evolutionary lineage of gene duplication, fusion, and finally functional degradation of a redundant pore by genetic drift in the eukaryotic homologues.

Other inferences emerging from these structures will require further testing to confirm or refute. First, a buried Na^+ ion occupying a unique position on the twofold axis invites us to view this cation as an intrinsic structural element stabilizing the dimer interface. Second, all four F^- ions observed in Bpe probably occupy the channel simultaneously, given their high occupancies (>80%) in the 2.1-Å structure, with B-factors matched to those in their coordination shells. The channel might therefore display multi-ion conduction phenomena akin to those long-known in K^+ channels25,26. Third, the channel's extreme F^- selectivity may arise from the narrow bore of the permeation pathway, which would exclude Cl^- ions while permitting the smaller F^- to enter. But this raises a key question: why would F^- enter that confined space? How does the protein compensate for the high energy of dehydrating F^-? We note that many of the coordinating groups are H-bond donors able to satisfy the F^- ion's H-bonding proclivities. While the unusual edge-on coordination by conserved phenylalanine rings is chemically intriguing, the energetic contributions of these interactions have not been established; nevertheless, in light of the conservation of these residues, we speculate that this short-range quadrupolar interaction contributes to F^- recognition and permeation in an essential way. The pore, though narrow, is lined with H-bonding residues and so could provide a polar conduit for the ion's journey across the membrane span.

A final point concerns the mechanism of electrodiffusive F^- transport through these oddly fashioned pores. The crucial role of N43 in permeation in Bpe and the confined crevice in which it resides lead us to conjecture that F^- moves along the pore concomitant with a rotameric switch of this side chain, such that the amide nitrogen remains H-bonded as the anion moves along the pore (Fig. 4). Thus, the conduction mechanism we offer here would be subtly distinct from classic diffusion through a fixed, water-filled channel. Instead, it would incorporate a central feature of membrane transporters – substrate transport coupled to concerted movement of the protein. An Asn side chain rotation could easily occur on the conduction timescale of microseconds, but formally this picture is a nuanced mix of electrodiffusion and configurational change – and so can be termed without apology a "channsporter" mechanism.

Methods

Biochemical

Expression, purification, and reconstitution of Fluc channels were as described in detail27,28. In the final purification step, Fluc protein was collected from a S200 size-exclusion column equilibrated in 100 mM NaF (or NaCl for zero-F^- preps), 10 mM Hepes pH 7.0, 5 mM n-decylmaltoside (DM). Bpe constructs carried two functionally neutral mutations to enhance expression, R29K/E94S or, for Hg labeling, R29K/E94C. Hg labeling was achieved by incubating Bpe with a 3-fold molar excess of Hg(II) acetate for 30 minutes between the Co-affinity and size exclusion columns. Ec2 constructs bore a single functionally neutral, expression-enhancing mutation, R25K, and, for selenomethionine incorporation, an additional methionine was introduced (A51M) to enhance phasing power. The C-terminal His_6 tag was removed from Bpe by treatment with lysine endoproteinase C (Roche)27, but was left on Ec2. Fluc protein was typically reconstituted into liposomes at low density (0.1-0.2 μg protein/mg lipid). For single-channel recording, liposomes were

fused into planar lipid bilayers in symmetrical solutions of 300 mM NaF, 15 mM MOPS, pH 7.0, and channels were recorded at 200 mV holding voltage27,29. Monobodies were expressed in E. coli and purified as described28. N-terminal His_6 tags were removed while bound to Talon beads by 16-hr treatment with TEV protease also carrying a His tag; monobodies with cleaved His tags were eluted from the affinity column with 150 mM NaCl, 40 mM Tris-HCl pH 7.5. For the final purification step, the preparation was passed over a S75 size exclusion column in 100 mM NaF (or NaCl), 10 mM HEPES pH 7. Monobodies were used immediately for crystallization or stored in frozen aliquots for channel-blocking experiments. For crystallization from detergent micelles, Fluc protein in solution containing 5 mM DM was concentrated to 10 mg/mL, a maneuver that concentrates the detergent 5-10-fold. Monobody solution (10 mg/mL) was supplemented with 4 mM DM immediately before mixing with channel in a 1.2:1 molar ratio. This protein solution was then mixed with an equal volume of crystallization solutions (0.5 μL for sitting drops in 96-well plates or 1 μL for hanging drops in 24-well plates). Bpe-S7 crystals grew in 3-5 days in crystallization solutions of 36-41% (w/v) polyethylene glycol 550 MME, 0.2 M $MgCl_2$ or $CaCl_2$, 0.1 M Tris, pH 8.5-8.9. Ec2-S9 crystals grew in 10-14 days in crystallization solutions containing 28-32% (w/v) polyethylene glycol 550 MME, 0.05 M $LiNO_3$, 0.1 M N-(2-Acetamido)iminodiacetic acid, pH 6.0-6.7. Crystals were frozen in liquid nitrogen for data collection. For lipidic cubic phase crystallization, Fluc protein concentrated to 10 mg/mL as above was dialyzed overnight to reduce the DM concentration to 10 mM. This was then mixed with monobody solution (10 mg/mL, with 4 mM DM) in a 1:1.2 molar ratio. The protein-laden mesophase was prepared by homogenizing 9.9 monoacylglycerol (monoolein) lipid with protein solution (10 mg/ml) at a weight ratio of 1:1.5 (protein:lipid) using a coupled syringe mixing device at 20°C30. Crystallization trials were carried out at 19°C in 96-well glass sandwich plates with 50 nl mesophase and 0.8 μl precipitant solution using an *in meso* robot. Crystallization solutions consisted of 22–26% (v/v) polyethylene glycol 500 DME, 0.1 M Na-citrate pH 5.5 +/- 10 mM NaF. Surfboard shaped crystals grew to a maximum size of 100 × 50 × 5 μm in 5-10 days. Wells were opened using a tungsten–carbide glasscutter, and the crystals were harvested using 50-100 μm micromounts (MiTeGen). Crystals were snap-cooled directly in liquid nitrogen prior to data collection on the Diamond Light Source beamlines I24 or I04.

Anion efflux from liposomes

Efflux of F^- or Cl^- out of liposomes was followed electrochemically as described31,36. Liposomes (10 mg lipid/mL, 0.2-1 μg protein/mg lipid) loaded with 300 mM KF or KCl solutions were freeze-thawed for 3 cycles and then extruded 21 times through a 400 nm filter. Immediately before the assay, a 100 μL sample was centrifuged through a 1.5-mL Sephadex column equilibrated with flux buffer (FB, 300 mM K-isethionate, 1 mM KF or KCl, 25 mM Hepes, pH 7) and was diluted 20-fold into a stirred chamber containing 3.8 mL FB. Halide concentration in the suspension was continuously monitored with a F^- or Cl^- electrode amplified through a pH meter and digitized at 5 Hz sampling frequency. Efflux was initiated by adding 1 μM valinomycin, and after several minutes 30 mM octylglucoside was added to obtain the 100% efflux level. Efflux rates were calculated after calibration with 25 μM additions of NaF or NaCl. For experiments with the Bpe N43D mutant, FB contained

an additional 100 mM Na-isethionate and 25 mM CHES buffer. Single-channel block by monobodies was recorded in planar phospholipid bilayers exactly as described28.

Structure Determination

Diffraction data for Bpe-S7 were processed by the Xia2 pipeline33 to XDS34 and scaled using aimless35. The space group was determined to be $P2_12_12$ with two Bpe dimers and four S7 monobodies in the asymmetric unit (Extended data Figure 1). A phasing strategy was devised that used pre-derivatisation of Bpe mutated with a single cysteine residue (E94C) with Hg (II) Acetate prior to crystallisation (see above). None of the native crystals were isomorphous with the Hg derivatised crystals (Riso > 40 %), despite having similar cell dimensions. Indeed, Hg derivatised crystals were observed to diffract X-rays to slightly higher resolution than native crystals, therefore effort was directed at these samples for phasing and refinement. The four Hg sites were located using the single wavelength anomalous dispersion (SAD) method as implemented in SHELX36 with the positions further refined and initial phases calculated using SHARP37 with solvent flattening in SOLOMON38. To improve the phases a second and third dataset were also collected at the Se edge using both Hg and seleno-L-methionine derivatized protein and another Hg derivatised dataset respectively (Extended Data Table 1). All 16 Se plus 4 Hg sites were located using SHELX and this dataset was combined with the initial 3.6 Angstrom Hg derivatized data. Phases were substantially improved using SIRAS combining the three datasets in SHARP. We did not observe higher resolution diffraction in the Native crystals, which typically gave diffraction between 3.6 - 3.8 Angstroms. Our highest resolution dataset with optimal scaling statistics was one of the Hg-derivatised crystals, we therefore used this dataset for subsequent refinement of the model built into the experimental electron density maps calculated from SHARP (see below). For the Bpe-L2 crystals, data were similarly processed and scaled in spacegroup P1. Phases were calculated using molecular replacement as implemented in PHASER39 using the experimentally determined Bpe model and a homology model of the L2 monobody using a previously determined structure of a loop-library monobody (PDB: 3RZW). The unambiguous solution showed two Bpe homodimers and four L2 monobodies. The electron density maps clearly showed major differences in the selected, variable regions of the monobody. For the Ec2-S9 crystals the data were processed as above with space group $P4_1$. Phases were calculated using Se-SAD with 8 Se sites, and processed as above. The experimental electron density maps were of exceptional quality following phase extension to the highest resolution shell of 2.58 Å. Data were collected at Advanced Light Source beamlines 8.2.1 and 8.2.2, and Diamond Light Source, beamlines I24 and I04.

Model building and refinement

For the Bpe-S7 complex structure, a model for the channel was built into the experimental electron density maps calculated from SHARP using O40 with sigma-A-weighted $2F_o$-F_c and mF_o-DF_c electron density maps. The S7 monobodies were initially built using a homology model based a previously determined structure of a side library monobody (PDB: 4JEG). These models were placed into the experimental electron density maps using MolRep41. The partial models were further cycled back into phase calculation in SHARP to improve the initial solvent envelope used for the solvent flipping procedure. The amino acid

side chains were then built using the Se and Hg sites to determine the correct register. Refinement of the Bpe-S7 model was carried out in Refmac542,43 against the highest resolution dataset for these crystals, 3.6 Å, which came from one of the Hg-derivatised crystals used for phasing (Extended Data Table 1). No prior phase information was used during the refinement, however refinement was improved following anisotropic truncation of the structure factors. To avoid biasing the model, NCS was not employed except at the final round of refinement to improve model geometry. Model validation was carried out using the Molprobity server44. The Ec2-S9 model was built directly into the experimental maps, using Se sites to ensure the correct register, and then monobodies were placed by molecular replacement using PHASER with a homology model based on S7. The Bpe-L2 model was built into the electron density maps calculated from PHASER following iterative rounds of structure refinement in PHENIX45 and Refmac5. The structural model was revised in real space with the program COOT46.

Extended Data

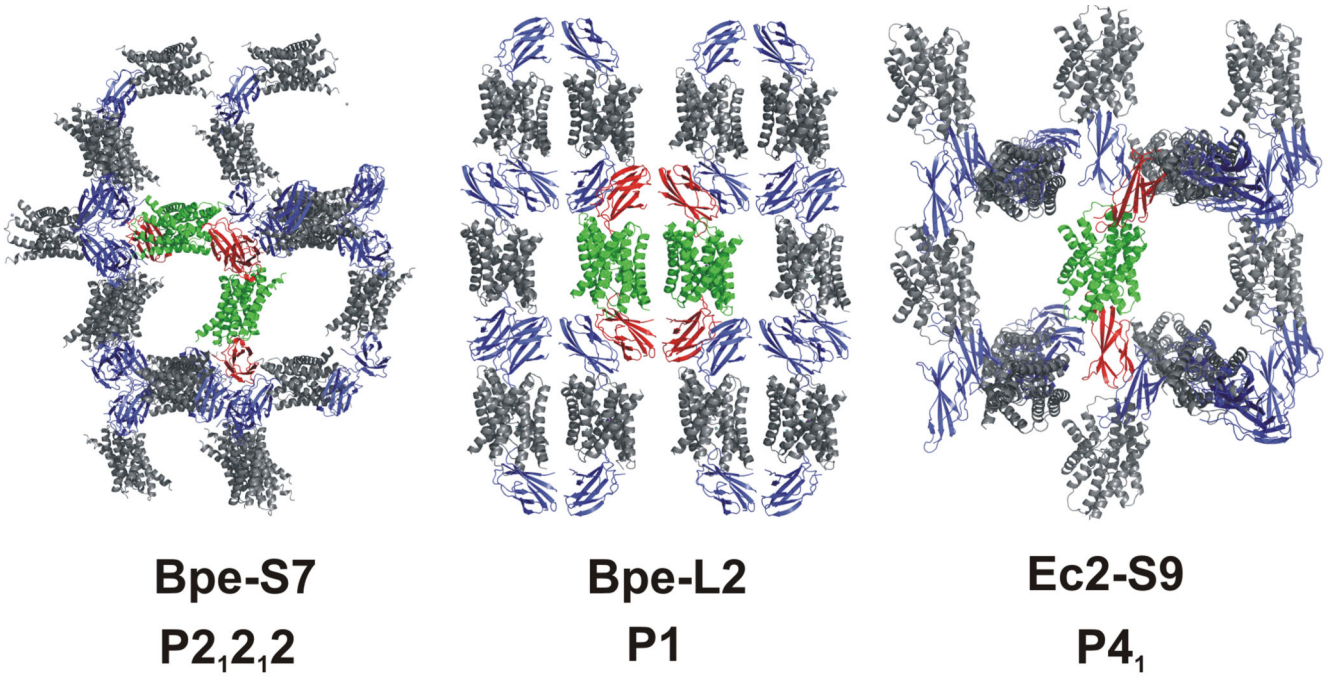

Extended Data Figure 1. Crystal lattices for the Bpe-S7, Bpe-L2 and Ec2-S9 crystal structures.
The asymmetric unit is shown in green and red (channel and monobody, respectively), and symmetry mates are shown in black and blue.

Europe PMC Funders Author Manuscripts

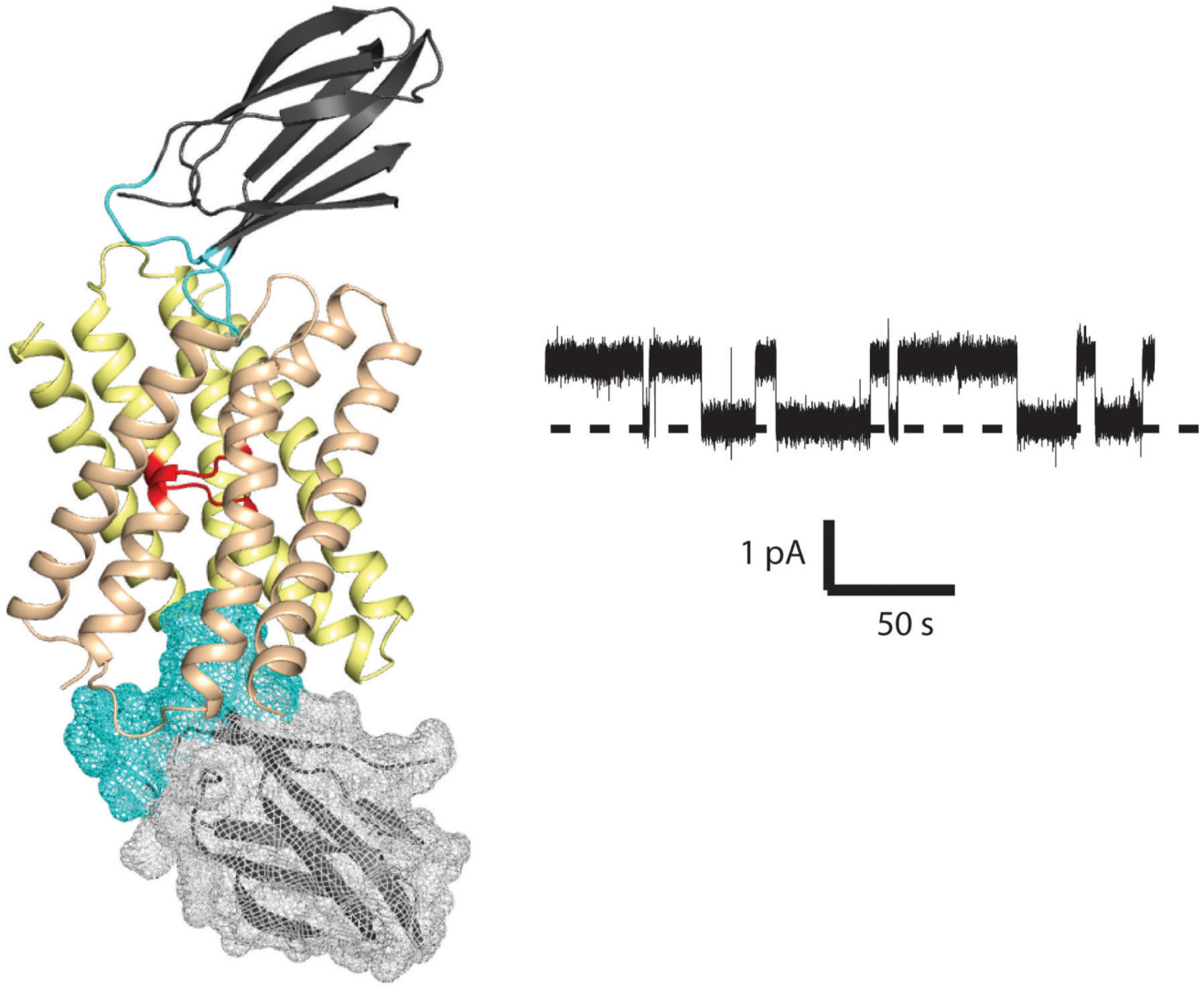

Extended Data Figure 2. Bpe-L2 complex.

Left panel: Cartoon schematic of Bpe crystal structure coloured as in Figure 1b. The variable regions of monobody L2 are colored cyan. Mesh rendering is shown for the lower monobody. Right panel: Single channel recording of Bpe in the presence of 200 nM L2. Zero-current level is indicated by the dashed line.

Europe PMC Funders Author Manuscripts

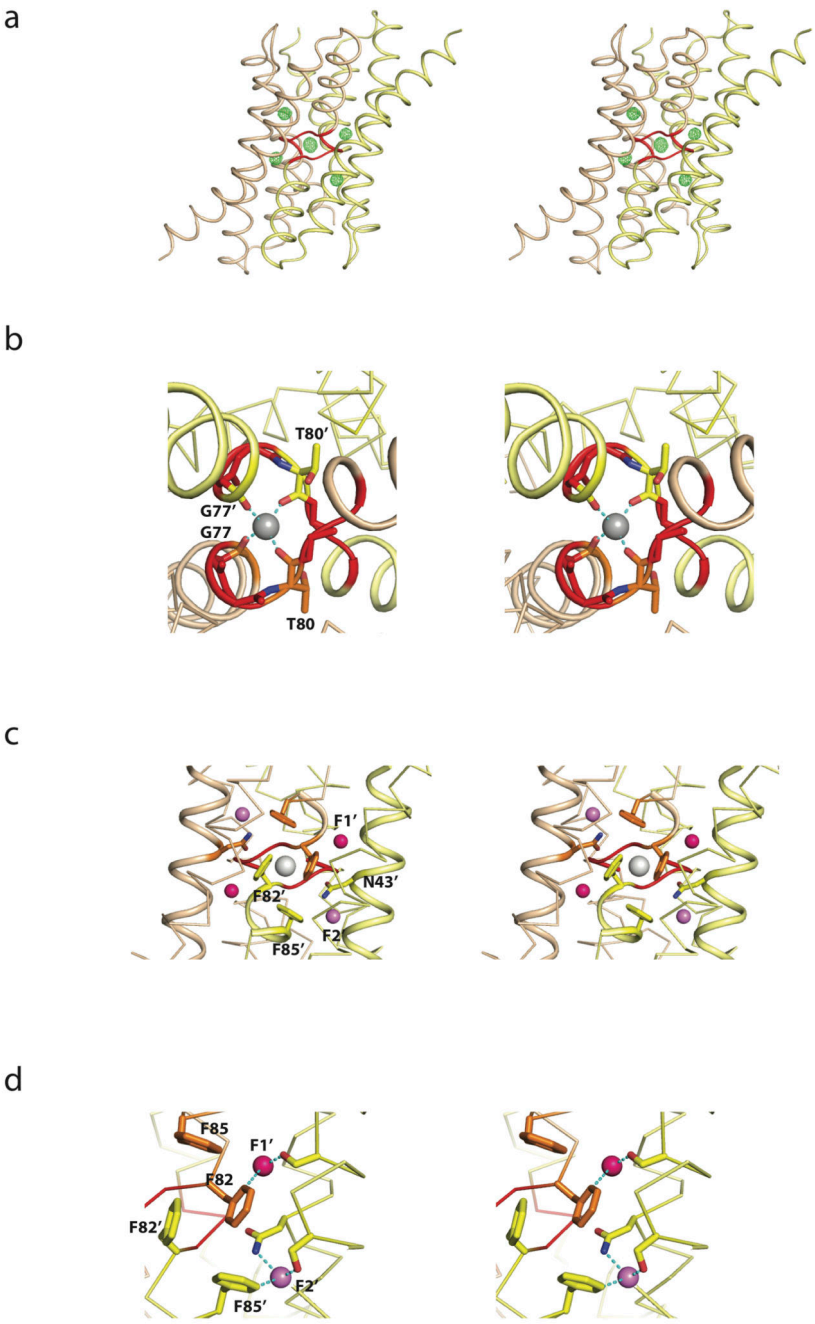

Extended Data Figure 3. Stereo images of Figure 2 a-d.

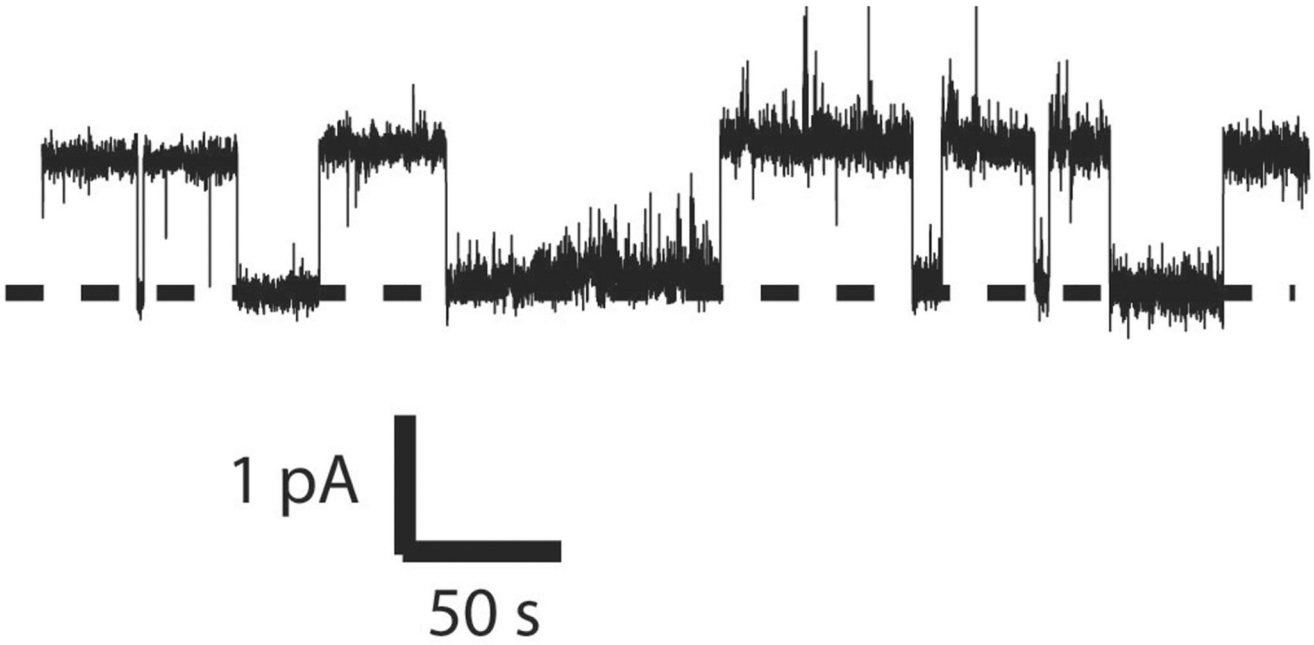

Extended Data Figure 4. Single channel trace of Bpe in Na^+-free recording solution, with addition of 200 nM blocking monobody L3.

Channels were recorded in the presence of 300 mM N-methyl-glucamine-fluoride, from which all small cations were rigorously excluded. The zero-current level is indicated by the dashed line.

Europe PMC Funders Author Manuscripts

Europe PMC Funders Author Manuscripts

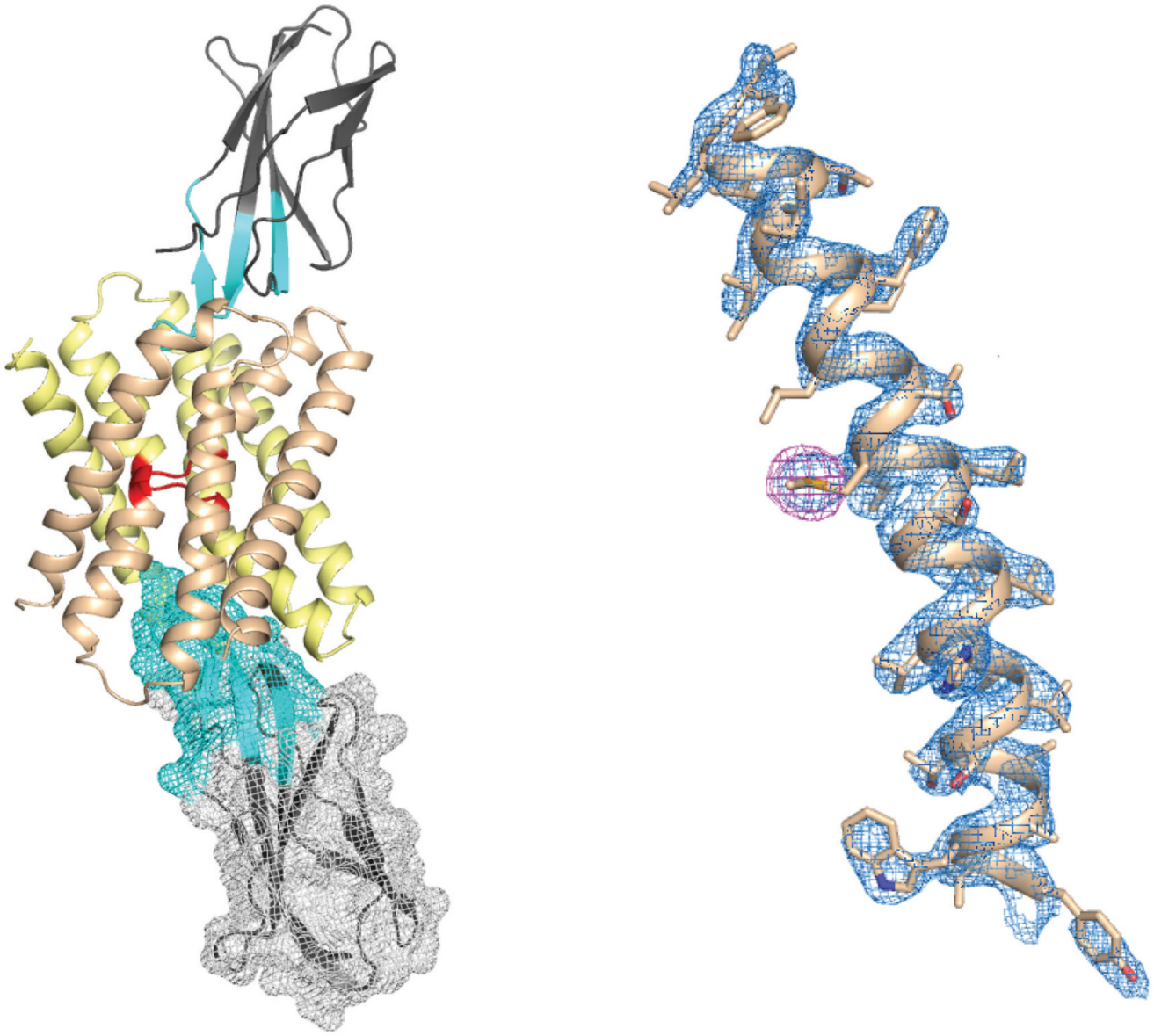

Extended Data Figure 5. Experimental electron density for the Ec2-S9 crystal structure.
Left panel: Cartoon schematic of Ec2 with S9 monobodies bound, coloured as Bpe in Figure 1b. Variable sequences of the monobodies (cyan) with ribbon or mesh representation. Right panel: Cartoon view of TM4 from Ec2, with the solvent flattened electron density map calculated from SHARP contoured at 1.8 sigma (blue), and anomalous difference density from seleno-L-methionine contoured at 5 sigma (magenta).

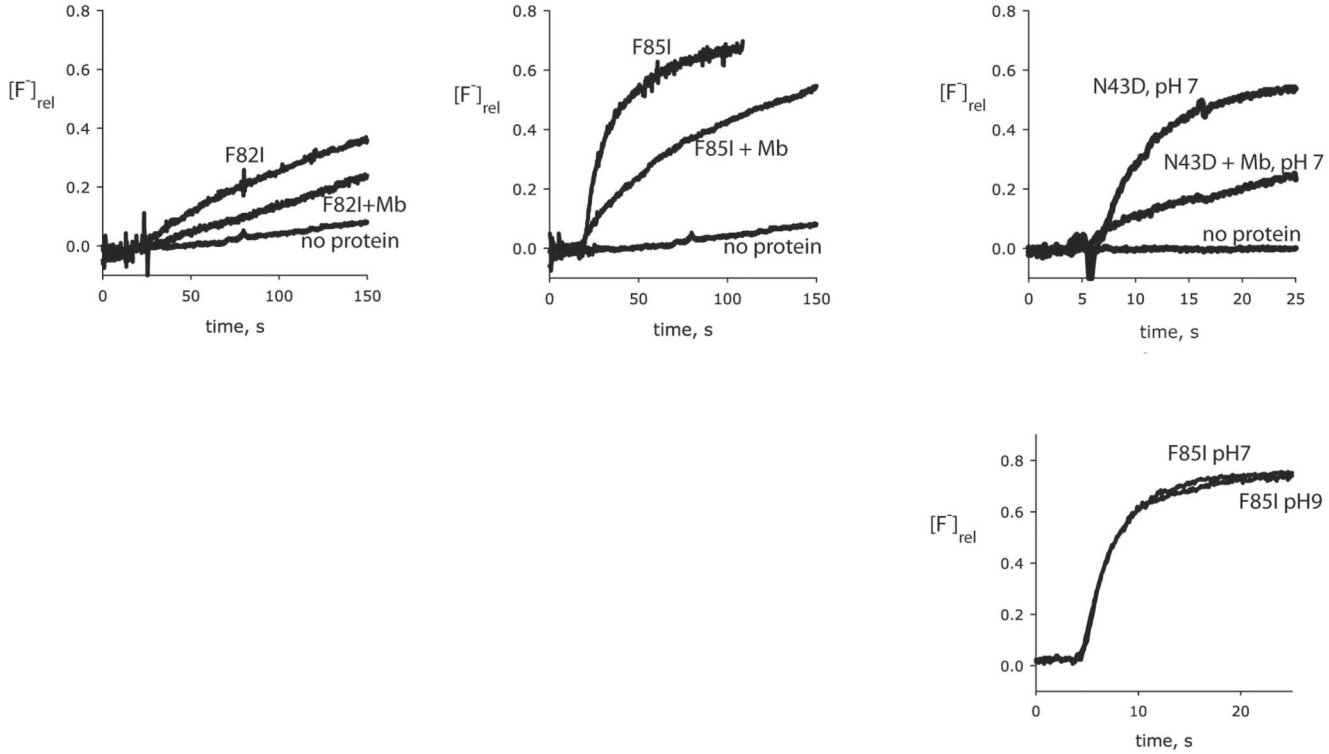

Extended Data Figure 6. Liposome flux assays of Bpe variants.

Upper three panels: F- transport from liposomes by Bpe mutants F82I, F85I, and N43D, in the presence and absence of 6 uM blocking monobody. F- efflux from proteoliposomes (0.2 μg protein/mg lipid for Phe mutants; 1 μg protein/mg lipid for N43D) was monitored with a F^- electrode and normalized against total trapped F^-. Lower panel: F^- dump by F85I measured at pH 7 and pH 9. Rates are summarized in Table S2.

Extended Data Figure 7. Sequence alignment of eukaryotic N- and C-terminal Fluc domain sequences, with bacterial homodimer sequences below.

Highly conserved residues are shaded in grey. For the eukaryotic sequences, residues expected to line “pore 2,” the pore mostly encompassed by the C-terminal domain, are colored red.

Europe PMC Funders Author Manuscripts

Europe PMC Funders Author Manuscripts

Extended Data Table 1

Data collection, phasing and refinement statistics for Bpe complexes

	Bpe-S7-Hg[1a]	Bpe-S7-Se	Bpe-S7- Hg[2]	Bpe-L2	Bpe-L2-no F	Ec2-S9-Se
Data collection						
Space group	$P2_12_12$	$P2_12_12$	$P2_12_12$	P1	P1	$P4_1$
Cell dimensions						
a, *b*, *c* (Å)	146.8, 183.7, 72.8	146.9, 184.0, 72.3	145.2, 185.0, 72.5	40.7, 83.9, 86.91	40.55, 84.59, 86.57	87.4, 87.4, 146.8
α, β, γ (°)	90, 90, 90	90, 90, 90	90, 90, 90	108.9, 96.9, 97.6	108.9, 101.4, 101.4	90, 90, 90
Resolution (Å)	48 – 3.6 (3.7 – 3.6)	48 – 3.6 (3.7 –3.6)	57 – 4.8 (4.7 – 4.8)	41 – 2.5 (2.5 – 2.1)	38 – 3.0 (3.1 – 3.0)	25-2.6 (2.7 – 2.6)
R_{merge}	8.8 (63.2)	15.2 (141)	12.7 (92.2)	8.8 (82.7)	12.9 (56.7)	17.4 (165)
Mn $I / \sigma I$	10.6 (2.6)	9.2 (1.7)	8.7 (2.9)	7.6 (1.3)	6.8 (2.0)	9.0 (1.9)
CC(1/2)[b]	99.8 (91.9)	99.8 (49.0)	99.9 (84.8)	99.4 (43.8)	97.2 (77.5)	--
Completeness (%)	99.6 (99.0)	98.7 (96.7)	99.7 (99.8)	96.8 (96.3)	92.1 (97.1)	99.9 (100)
Redundancy	6.3 (6.7)	6.4 (6.2)	6.0 (6.1)	3.4 (3.4)	3.3 (3.4)	14.3 (14.3)
R_{cullis} (%)	-- / 96.0	45.8 / 96.0	93.0 / 99.0			87.9
Isomorphous / Anomalous						
Phasing Power[c]	-- / 0.323	1.032 / 0.501	0.338 / 0.073			0.825
Isomorphous / Anomalous						
Refinement						
Resolution (Å)	114.7 – 3.6			40.9 – 2.1	38.1 – 3.0	24.2 – 2.6
No. reflections	21,085			51,555	16732	34,593
R_{work} / R_{free}	23.6 / 26.9			20.5 / 24.0	34.0 / 39.8	22.4 / 26.4
Ramachandran Favored	85.4			96.5	95.7	92.6
Ramachandran Outliers	4.02			3.04	0.6	2.53
R.m.s. deviations						
Bond lengths (Å)	0.011			0.009	0.014	0.009
Bond angles (°)	1.53			1.26	1.59	1.50

[a] For details on derivatisation see Supplementary Information

[b] Mn (I) half-set correlation as reported by Aimless

[c] Phasing Power = rms ($|F_H|$ / ((F_H + F_P)-(F_{PH})))

Extended Data Table 2
F^- turnover rate for Bpe mutants[1]

Mutant	rate (s^{-1})
WT[2]	~3x10^5
N43D, pH 6.5	4330 ± 440
N43D, pH 7	1860 ± 210
N43D, pH 7 + Mb	210 ± 30
N43D, pH 9	undetectable
F82I	200 ± 12
F82I + Mb	45 ± 7
F85I	1950 ± 200
F85I + Mb	300 ± 25
F85I, pH 9	1680 ± 110

[1] Analogous experiments in which Cl^- efflux was measured gave no detectable activity in any samples.

[2] Estimated based on single channel currents. F^- turnover by WT exceeds response time of the electrode.

Each value represents mean ± s.e. of 3 determinations calculated from initial efflux rate.

Acknowledgements

We are grateful to Jo Parker for critically reading the manuscript, to Dan Turman, Ashley Lajoie, Minh Pham, and Kene Piasta for pilot experiments, to Scott Strobel for sharing results of unpublished experiments, and to Bruce Foxman for help with the Cambridge Structural Database. This work was supported in part by Wellcome Trust Investigator Award 102890/Z/13/Z and NIH grants RO1-GM107023 and U54-GM087519. RBS was supported by NIH grant K99-GM-111767. CM is grateful to Dr Frances Ashcroft and Lincoln College, Oxford for hosting a Newton-Abraham Visiting Professorship

References

1. Baker JL, et al. Widespread genetic switches and toxicity resistance proteins for fluoride. Science. 2012; 335:233–235. [PubMed: 22194412]
2. Li S, et al. Eukaryotic resistance to fluoride toxicity mediated by a widespread family of fluoride export proteins. Proc Natl Acad Sci U S A. 2013; 110:19018–19023. DOI: 10.1073/pnas.1310439110 [PubMed: 24173035]
3. Ji C, Stockbridge RB, Miller C. Bacterial fluoride resistance, Fluc channels, and the weak acid accumulation effect. J Gen Physiol. 2014; 144:257–261. DOI: 10.1085/jgp.201411243 [PubMed: 25156118]
4. Smith KD, et al. FEX1 is a constitutively expressive fluoride channel in *Saccaromyces cerevisiae* with functional asymmetry of its two homologous domains. J Biol Chem. 2015; 1:1–2.
5. Stockbridge RB, Robertson JL, Kolmakova-Partensky L, Miller C. A family of fluoride-specific ion channels with dual-topology architecture. eLife. 2013; 2:e01084.doi: 10.7554/eLife.01084 [PubMed: 23991286]
6. Stockbridge RB, Koide A, Miller C, Koide S. Proof of dual-topology architecture of Fluc F− channels with monobody blockers. Nat Commun. 2014; 5doi: 10.1038/ncomms6120
7. Adamek E, Pawlowska-Goral K, Bober K. In vitro and in vivo effects of fluoride ions on enzyme activity. Annales Academiae Medicae Stetinensis. 2005; 51:69–85. [PubMed: 16519100]
8. Stockbridge RB, et al. Fluoride resistance and transport by riboswitch-controlled CLC antiporters. Proc Natl Acad Sci U S A. 2012; 109:15289–15294. DOI: 10.1073/pnas.1210896109 [PubMed: 22949689]

9. Ubarretxena-Belandia I, Baldwin JM, Schuldiner S, Tate CG. Three-dimensional structure of the bacterial multidrug transporter EmrE shows it is an asymmetric homodimer. The EMBO journal. 2003; 22:6175–6181. DOI: 10.1093/emboj/cdg611 [PubMed: 14633977]
10. Schuldiner S. EmrE, a model for studying evolution and mechanism of ion-coupled transporters. Biochim Biophys Acta. 2009; 1794:748–762. [PubMed: 19167526]
11. Morrison EA, et al. Antiparallel EmrE exports drugs by exchanging between asymmetric structures. Nature. 2012; 481:45–50. [PubMed: 22178925]
12. Miller C. Open-state substructure of single chloride channels from *Torpedo* electroplax. Phil Trans Roy Soc B. 1982; 299:401–411. [PubMed: 6130538]
13. Rapp M, Granseth E, Seppala S, von Heijne G. Identification and evolution of dual-topology membrane proteins. Nat Struct Mol Biol. 2006; 13:112–116. [PubMed: 16429150]
14. Koide A, Wojcik J, Gilbreth RN, Hoey RJ, Koide S. Teaching an old scaffold new tricks: monobodies constructed using alternative surfaces of the FN3 scaffold. J Mol Biol. 2012; 415:393–405. [PubMed: 22198408]
15. Turman DL, Nathanson JT, Stockbridge RB, Street TO, Miller C. Two-sided block of a dual-topology F^- channel. Proc Natl Acad Sci USA. 2015 in press.
16. Harding MM. Metal-ligand geometry relevant to proteins and in proteins: sodium and potassium. Acta Crystallogr D Biol Crystallogr. 2002; 58:872–874. [PubMed: 11976508]
17. Varma S, Sabo D, Rempe SB. K^+/Na^+ selectivity in K channels and valinomycin: over-coordination versus cavity-size constraints. J Mol Biol. 2008; 376:13–22. [PubMed: 18155244]
18. Lev, B.; R, B.; Noskov, SY. Encyclopedia of Metalloproteins. Uversky, VN., editor. Springer; 2013. p. 2112-2118.
19. Philip V, et al. A survey of aspartate-phenylalanine and glutamate-phenylalanine interactions in the protein data bank: searching for anion-pi pairs. Biochemistry. 2011; 50:2939–2950. DOI: 10.1021/bi200066k [PubMed: 21366334]
20. Allen FH. The Cambridge Structural Database: a quarter of a million crystal structures and rising. Acta crystallographica Section B, Structural science. 2002; 58:380–388. [PubMed: 12037359]
21. Dickson V, Pedi L, Long SB. Structure and insights into the function of a Ca^{2+}-activated Cl^- channel. Nature. 2014; 516:213–218. DOI: 10.1038/nature13913 [PubMed: 25337878]
22. Walden M, et al. Uncoupling and turnover in a Cl^-/H^+ exchange transporter. J Gen Physiol. 2007; 129:317–329. [PubMed: 17389248]
23. Brammer AE, Stockbridge RB, Miller C. F-/Cl- selectivity in CLCF-type F-/H+ antiporters. J Gen Physiol. 2014; 144:129–136. DOI: 10.1085/jgp.201411225 [PubMed: 25070431]
24. Weinreich F, Jentsch TJ. Pores formed by single subunits in mixed dimers of different CLC chloride channels. J Biol Chem. 2001; 276:2347–2353. [PubMed: 11035003]
25. Hille B, Schwarz W. Potassium channels as multi-ion single-file pores. J Gen Physiol. 1978; 72:409–442. [PubMed: 722275]
26. Morais-Cabral JH, Zhou Y, MacKinnon R. Energetic optimization of ion conduction rate by the K+ selectivity filter. Nature. 2001; 414:37–42. [PubMed: 11689935]
27. Stockbridge RB, Robertson JL, Kolmakova-Partensky L, Miller C. A family of fluoride-specific ion channels with dual-topology architecture. eLife. 2013; 2:e01084.doi: 10.7554/eLife.01084 [PubMed: 23991286]
28. Stockbridge RB, Koide A, Miller C, Koide S. Proof of dual-topology architecture of Fluc F− channels with monobody blockers. Nat Commun. 2014; 5doi: 10.1038/ncomms6120
29. Turman DL, Nathanson JT, Stockbridge RB, Street TO, Miller C. Two-sided block of a dual-topology F^- channel. Proc Natl Acad Sci USA. 2015 in press.
30. Caffrey M, Cherezov V. Crystallizing membrane proteins using lipidic mesophases. Nature protocols. 2009; 4:706–731. DOI: 10.1038/nprot.2009.31 [PubMed: 19390528]
31. Walden M, et al. Uncoupling and turnover in a Cl^-/H^+ exchange transporter. J Gen Physiol. 2007; 129:317–329. [PubMed: 17389248]
32. Brammer AE, Stockbridge RB, Miller C. F-/Cl- selectivity in CLCF-type F-/H+ antiporters. J Gen Physiol. 2014; 144:129–136. DOI: 10.1085/jgp.201411225 [PubMed: 25070431]

33. Winter G, Lobley CM, Prince SM. Decision making in xia2. Acta Crystallogr D Biol Crystallogr. 2013; 69:1260–1273. DOI: 10.1107/S0907444913015308 [PubMed: 23793152]
34. Kabsch W. Xds. Acta Crystallogr D Biol Crystallogr. 2010; 66:125–132. DOI: 10.1107/S0907444909047337 [PubMed: 20124692]
35. Evans PR. An introduction to data reduction: space-group determination, scaling and intensity statistics. Acta Crystallogr D Biol Crystallogr. 2011; 67:282–292. DOI: 10.1107/S090744491003982X [PubMed: 21460446]
36. Sheldrick GM. A short history of SHELX. Acta Crystallogr A. 2008; 64:112–122. [PubMed: 18156677]
37. Bricogne G, et al. Generation, representation and flow of phase information in structure determination: recent developments in and around SHARP 2.0. Acta Crystallogr D Biol Crystallogr. 2003; 59:2023–2030. [PubMed: 14573958]
38. Abrahams JP, Leslie AG. Methods used in the structure determination of bovine mitochondrial F1 ATPase. Acta Crystallogr D Biol Crystallogr. 1996; 52:30–42. DOI: 10.1107/S0907444995008754 [PubMed: 15299723]
39. McCoy AJ, et al. Phaser crystallographic software. Journal of applied crystallography. 2007; 40:658–674. DOI: 10.1107/S0021889807021206 [PubMed: 19461840]
40. Jones TA, Zou JY, Cowan SW, Kjeldgaard M. Improved methods for building protein models in electron density maps and the location of errors in these models. Acta crystallographica Section A, Foundations of crystallography. 1991; 47(Pt 2):110–119. [PubMed: 2025413]
41. Vagin A, Teplyakov A. Molecular replacement with MOLREP. Acta Crystallogr D Biol Crystallogr. 2010; 66:22–25. DOI: 10.1107/S0907444909042589 [PubMed: 20057045]
42. Murshudov GN, et al. REFMAC5 for the refinement of macromolecular crystal structures. Acta Crystallogr D Biol Crystallogr. 2011; 67:355–367. [PubMed: 21460454]
43. Collaborative Computational Project, Number 4. Acta Crystallogr D Biol Crystallogr. 2011; 67:235–242. [PubMed: 21460441]
44. Chen VB, et al. Molprobity: all-atom structure validataion for macromolecular crystallography. Acta Crystallogr D Biol Crystallogr. 2010; 66:12–21. [PubMed: 20057044]
45. Adams PD, et al. PHENIX: a comprehensive Python-based system for macromolecular structure solution. Acta Crystallogr D Biol Crystallogr. 2010; 66:213–221. DOI: 10.1107/S0907444909052925 [PubMed: 20124702]
46. Emsley P, Lohkamp B, Scott WG, Cowtan K. Features and development of Coot. Acta Crystallogr D Biol Crystallogr. 2010; 66:486–501. DOI: 10.1107/S0907444910007493 [PubMed: 20383002]

Europe PMC Funders Author Manuscripts

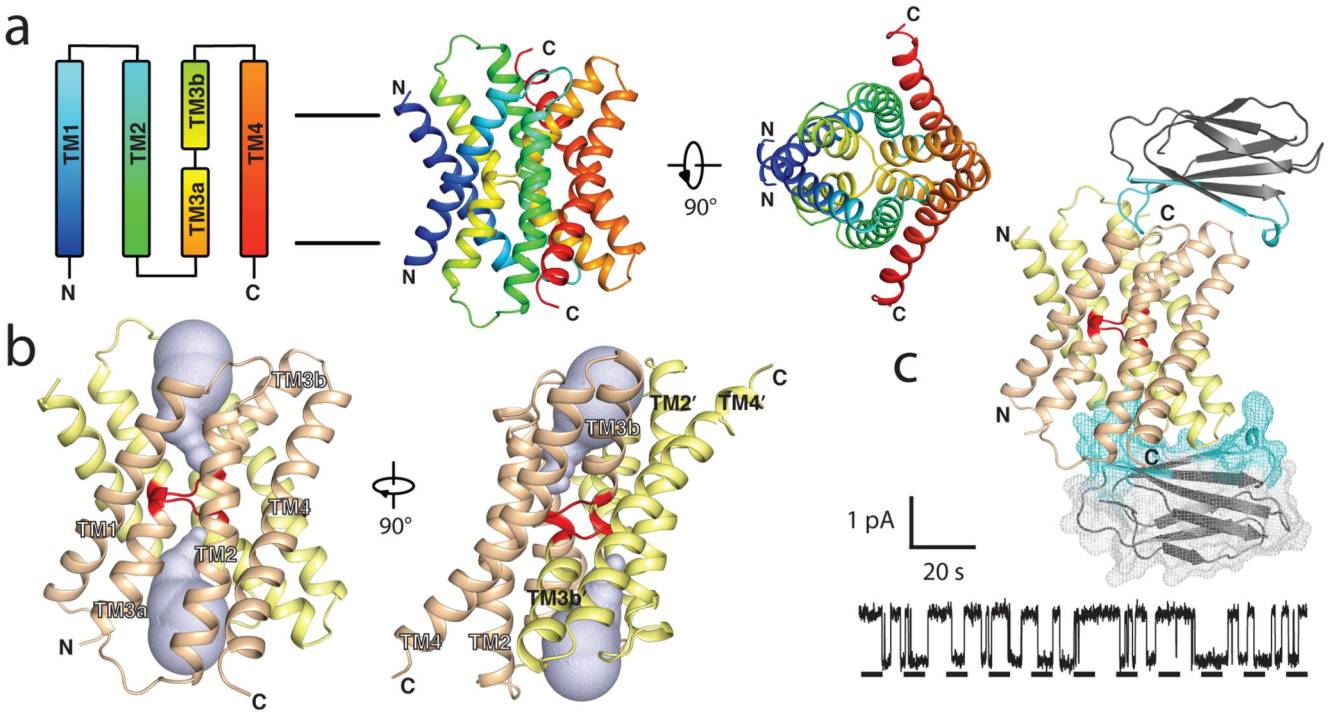

Figure 1. Bpe-S7 structure.

a. Bpe homodimer, viewed parallel (center panel) and perpendicular (right panel) to the membrane. Coloring as in TM helix schematic at left. **b.** Through-membrane views, indicating TM3 break (red) and the aqueous volume within the vestibules (blue). **c.** Bpe with S7 monobodies bound. Variable sequences of the monobodies (cyan) with ribbon or mesh representation. Single-channel Bpe recording showing S7 (500 nM) binding and dissociation. Zero-current level indicated by the dashed line.

Europe PMC Funders Author Manuscripts

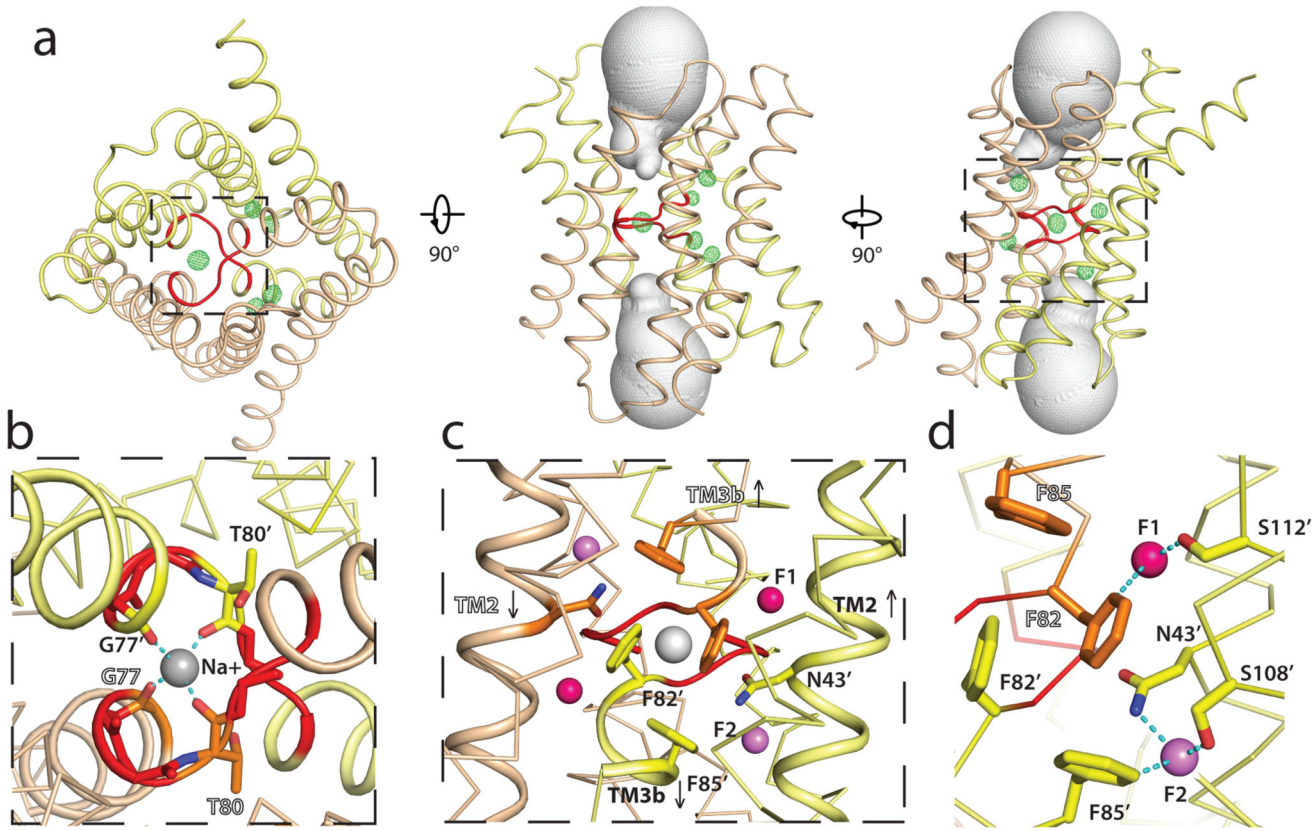

Figure 2. Bpe-L2 structure.

a. Bpe homodimer with mFo-DFc map contoured at 4σ (green), viewed from solution (left) and the membrane (center, right). Aqueous volume of the vestibules are shown (gray). Dashed boxes indicate zoomed regions in panels b, c. **b.** Na^+ coordination sphere viewed from solution. TM3 is represented as a cartoon. **c**. 90° view showing Na^+, F^- ions, N43, and the phenylalanine box (F82 and F85). Cartoons indicate TM2, TM3. **d.** F^- coordination shells, with F82, S112 (F1), N43, S108, and F85 (F2) shown as sticks. Stereo images are shown in Extended Data Fig. 3.

Europe PMC Funders Author Manuscripts

Europe PMC Funders Author Manuscripts

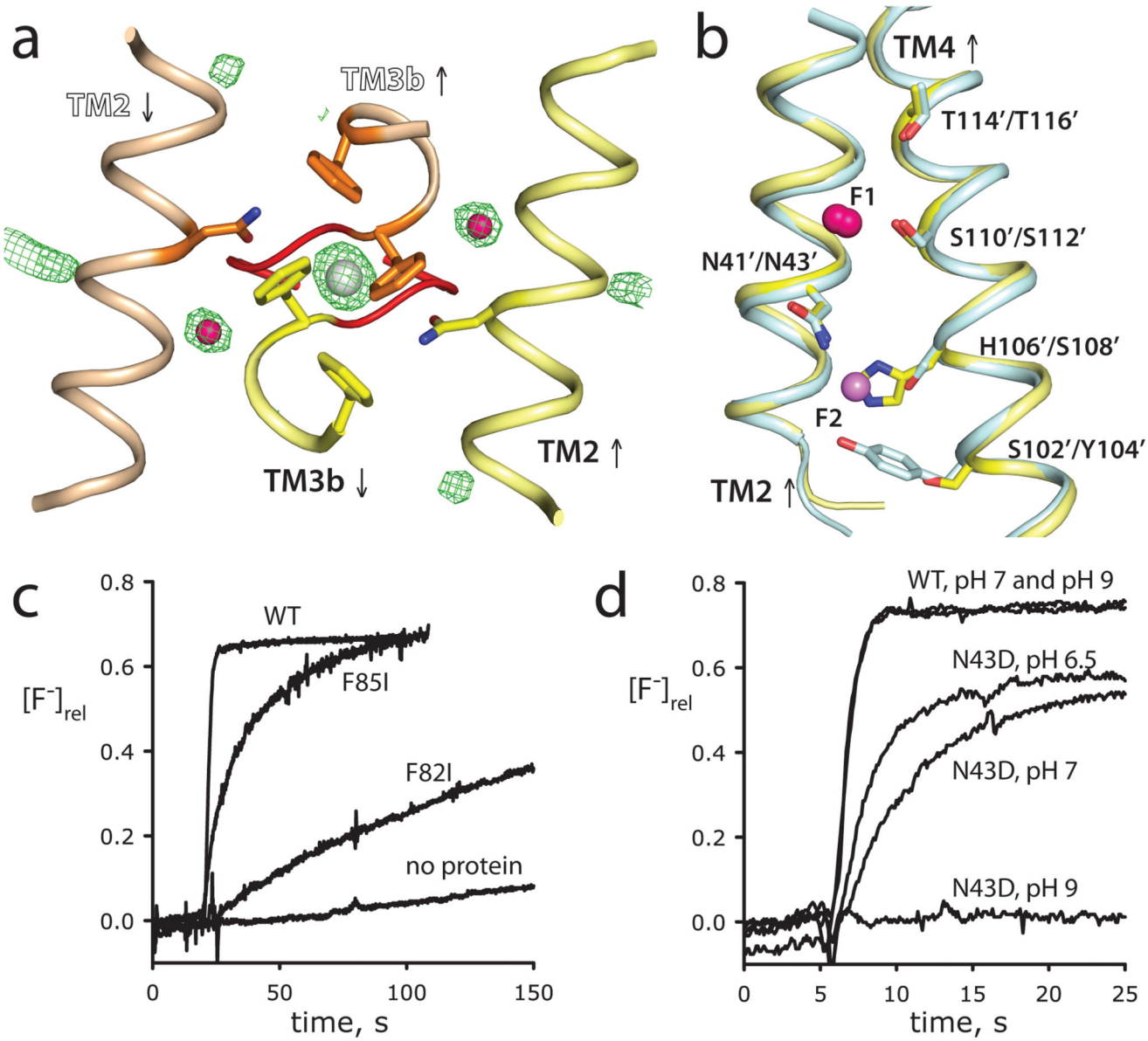

Figure 3. Identification of F⁻ ions.

a. Ec2-S9 F⁻-binding region, analogous to Fig. 2c, with mFo-DFc map contoured at 4.8 σ and ion positions shown. The phenylalanine box and N41 are shown as sticks. Weak densities in F2 regions could not be unambiguously assigned. **b.** Overlay of TM2 and TM4 from Bpe-L2 (cyan) and Ec2-S9 (yellow) structures, showing F⁻ ions and polar track. **c., d.** Functional consequences of mutating F⁻-coordinating residues. F⁻ efflux from Bpe-reconstituted proteoliposomes, initiated with valinomycin and monitored with a F⁻ electrode, reported relative to total F⁻ trapped in liposomes.

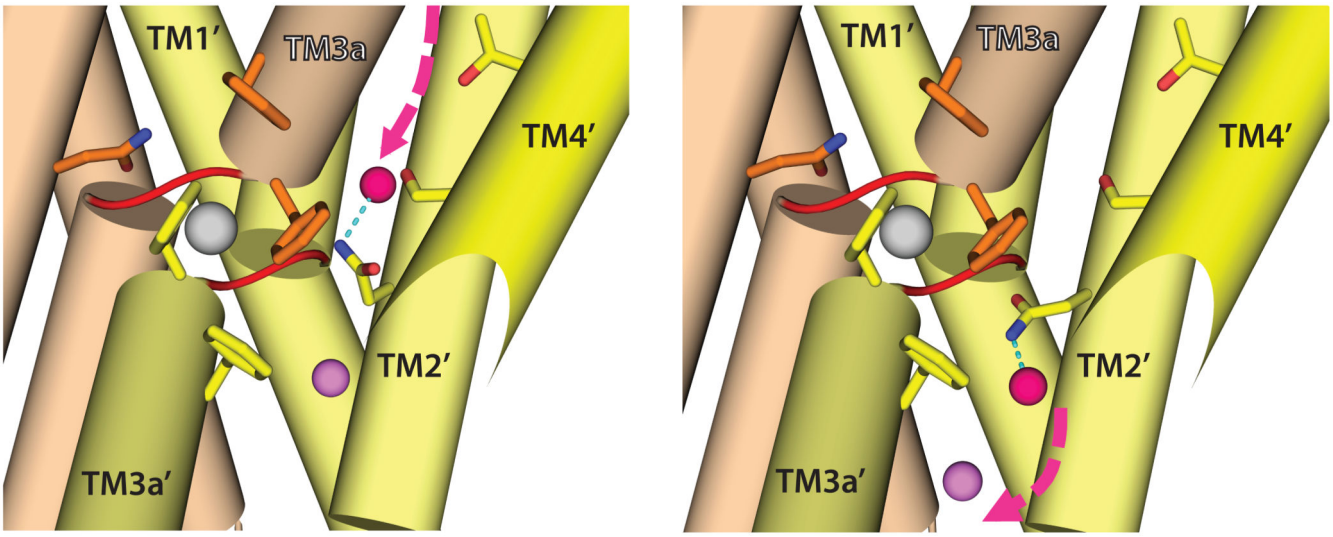

Figure 4. Model of F^- movement by Fluc channsporter mechanism.

The two panels show proposed successive steps of F^- ion electrodiffusion through a two-ion pore being facilitated by the concerted rotation of N43 sidechain. The lower half of the TM4 polar track is removed for clarity.

Europe PMC Funders Author Manuscripts